Tingting Zhu
Mechanical and Industrial Engineering,
Northeastern University,
Boston, MA 02115

Guangxu Li[1]
Mechanical and Industrial Engineering,
Northeastern University,
Boston, MA 02115

Sinan Müftü
Mechanical and Industrial Engineering,
Northeastern University,
Boston, MA 02115

Kai-tak Wan[2]
Mechanical and Industrial Engineering,
Northeastern University,
Boston, MA 02115

Revisiting the Constrained Blister Test to Measure Thin Film Adhesion

A thin film is clamped at the periphery to form a circular freestanding diaphragm before a uniform pressure, p, is applied to inflate it into a blister. The bulging membrane adheres to a rigid constraining plate with height, w_0, from the nondeformed membrane. Increasing pressure expands the contact circle of radius, c. Depressurization causes shrinkage of the contact and "pull-off" or spontaneous detachment from the plate. Simultaneous measurement of (p, w_0, c) allows one to determine the adhesion energy, γ. A solid mechanics model is constructed based on small strain and linear elasticity, which shows a characteristic loading–unloading hysteresis. The results are consistent with a large deformation model in the literature. [DOI: 10.1115/1.4036776]

Keywords: membrane, adhesion, delamination, constrained blister, pull-off

1 Introduction

Thin film adhesion has significant impacts in nanotechnology and life sciences. Dannenberg [1] introduced the classical blister test where a uniform pressure drives an axisymmetric delamination of a coating from a rigid substrate. The work of adhesion is then determined by the contact radius as a function of the applied pressure. A notorious shortcoming of the method is the catastrophic crack propagation at onset of delamination. A number of alternative methods are available in the literature, including the expansion of a fixed mass of gas at the film–substrate interface when the sample is exposed to an external vacuum [2] or elevated temperature [3]. Dillard and coworkers [4–7] introduced the constrained blister test by restricting the blister height using a rigid planar plate, thus stabilizing the delamination under a constant pressure. A "modified" constrained blister [8,9] pressurizes a freestanding membrane clamped at the periphery until the membrane makes adhesive contact with the constraining plate (Fig. 1). The modified test belongs to "confined delamination" where the contact circle is bounded by the diaphragm dimension [10]. Plaut et al. [9] extended the work to include short-range to long-range intersurface attraction based on linear elasticity. Xu and Liechti [11] adopted the modified method to investigate structured acrylate layers on a polyethylene terephthalate carrier film. Flory et al. [12] experimentally investigated the adhesion of a pressurized elastomeric film on a planar substrate. The measurement was later analyzed by Long et al. [13,14] based on large deformation using rubber hyperelasticity.

In this paper, a solid-mechanics model for the constrained blister is based on small strain approximation, linear elasticity, and zero-range surface force. The loading–pressurization and unloading–depressurization process are investigated, along with the critical events such as "pull-off" or spontaneous detachment of film from the substrate. The interrelations between the measurable quantities of blister height, applied pressure, and contact radius are derived. These functions will be useful to the experimentalists. Rigorous comparison with the existing theoretical models are made in Sec. 3.

2 Theoretical Model

Figure 1 shows a linear elastic, thin, freestanding, planar membrane with radius, a, thickness, h, elastic modulus, E, and Poisson's ratio, ν, clamped at its periphery. It is initially free of residual stress and possesses a negligible flexural rigidity. The deformation is therefore dominated by membrane stretching with negligible plate bending. A rigid plate is placed at a distance, w_0, from the substrate to restrict the blister height. A uniform pressure, p, is applied to form a free bulging blister. Further increase in p causes the membrane to adhere to the constraining plate, making a contact circle with radius, c, contact angle, θ, and deformed annular profile of $w(r)$. A force F exerting on the plate maintains the desirable w_0. Upon depressurization, simultaneous measurements of p and c allow the adhesion energy, γ, to be deduced. A thermodynamic energy balance based on small elastic strain approximation is used to derive the adhesion–detachment trajectory. Table 1 lists all the physical (bold) and normalized (plain) variables to be used hereafter.

2.1 Mechanical Response With a Fixed Contact Circle.

Before addressing the adhesion mechanics, it is necessary to first derive the mechanical response for an annulus with fixed inner and outer radii based on Williams' average stress approximation for small strain and small debonding angle [8]. Figure 1 shows a

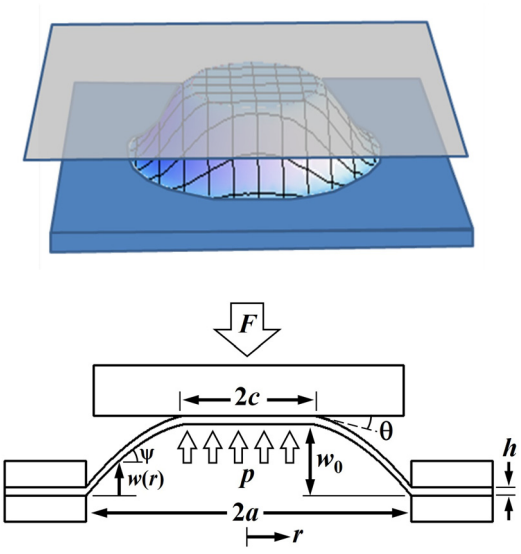

Fig. 1 Schematic of a constrained blister test with the membrane adhering to the constraining plate

[1]Present address: Texas Instruments, Dallas, TX.
[2]Corresponding author.
Contributed by the Applied Mechanics Division of ASME for publication in the Journal of Applied Mechanics. Manuscript received April 2, 2017; final manuscript received May 13, 2017; published online May 31, 2017. Editor: Yonggang Huang.

freestanding annulus ($\boldsymbol{c} < \boldsymbol{r} \le \boldsymbol{a}$) inclining at a small angle $\boldsymbol{\psi} \approx \partial \boldsymbol{w}/\partial \boldsymbol{r}$ to the horizon. Balancing vertical forces

$$\boldsymbol{\pi r^2 p} - \boldsymbol{F} = 2\boldsymbol{\pi r} \times \boldsymbol{\sigma h} \times \sin \boldsymbol{\psi} \approx 2\boldsymbol{\pi r} \times \boldsymbol{\sigma h} \times \boldsymbol{\psi} \tag{1}$$

where $\boldsymbol{\sigma}$ is the average membrane stress in the annulus. Rearrangement of Eq. (1) yields

$$\psi(r) = \frac{p}{\sigma} \times \left(r - \frac{\Phi}{r} \right) \tag{2}$$

with the loading ratio, $\Phi = \boldsymbol{F}/(\pi \boldsymbol{a}^2 \boldsymbol{p}) = F/p$. Note that $\Phi \le 1$ if delamination at all occurs. When the membrane is in full contact with the substrate with $w_0 = 0$, $\Phi = 1$. When $\theta = 0$, the load is fully supported by the applied pressure, and Eq. (1) requires $\Phi = c^2$. At $r = c$, the debonding angle at the contact edge becomes

$$\theta = \psi(c) = \frac{p}{\sigma} \times \left(c - \frac{\Phi}{c} \right) \tag{3}$$

and the annular profile

$$w(r) = \int_r^1 \psi . dr = \frac{p}{2\sigma} \times \left[1 - r^2 - \Phi \times \log\left(\frac{1}{r^2} \right) \right] \tag{4}$$

with the blister height, or, plate-substrate gap

$$w_0 = w(c) = \frac{p}{2\sigma} \times \left[1 - c^2 - \Phi \times \log\left(\frac{1}{c^2} \right) \right] \tag{5}$$

To obtain the membrane stress, a radial element with radius, $\boldsymbol{r}$, and width, $d\boldsymbol{r}$, is stretched to an elongated length of $d\boldsymbol{r} \times \sec \boldsymbol{\psi}$. For $\boldsymbol{\psi} \approx 0$, the linear engineering strain is approximated by $\boldsymbol{\varepsilon}_{\text{linear}} = \sec \boldsymbol{\psi} - 1 \approx \boldsymbol{\psi}^2/2 \approx (d\boldsymbol{w}/d\boldsymbol{r})^2/2$. The average linear strain over the annulus ($\boldsymbol{c} < \boldsymbol{r} < \boldsymbol{a}$) is given by

$$\boldsymbol{\varepsilon} = \frac{1}{2} \times \left[\int_c^a \frac{\boldsymbol{\psi}^2}{2} \cdot 2\pi \boldsymbol{r} d\boldsymbol{r} \Big/ \int_c^a 2\pi \boldsymbol{r} d\boldsymbol{r} \right] \tag{6}$$

The square bracket is the average biaxial areal strain over the freestanding annulus, and the factor of 1/2 reduces the 2D strain to 1D. The average membrane stress, $\boldsymbol{\sigma} = \boldsymbol{E}.\ \boldsymbol{\varepsilon}$, is given by

$$\sigma = \left(\frac{3}{2} \right)^{1/3} \times p^{2/3} \times \left(1 + c^2 - 4\Phi + 2\frac{\Phi^2}{\zeta^2} \right)^{1/3} \tag{7}$$

with $\zeta^2 = (1 - c^2)/\log(c^{-2})$. Elimination of σ from Eqs. (5) and (7) leads to the mechanical response

$$p = 12 w_0^3 \times \left\{ \frac{1 + c^2 - 4\Phi + 2\Phi^2 \zeta^{-2}}{(1 - c^2)(1 - \Phi\zeta^{-2})} \right\} \tag{8}$$

which is a cubic relation, $p \propto w_0^3$, for a constant c.

2.2 Loading by Pressurization. The constraining plate is fixed at $w_0 = 1$. A uniform pressure is applied to drive a blister. Figure 2 shows $c(p)$, $\theta(p)$, and $F(p)$, while Fig. 3 shows the corresponding changing blister profile as a function of applied pressure. Initial loading proceeds along path OA where the blister is yet to make contact with the plate and $c = 0$ always. An elastic strain gradually builds up upon loading. A free expanding blister is governed by $p = 12 w_0^3$ by substituting $c = 0$ and $\Phi = 0$ in Eq. (8). At A, the applied pressure reaches a critical threshold $p_A = 12$, and the blister makes a point contact with the plate. Further increase in p proceeds along path AB, flattens the blister at the plate, expands the contact circle, and raises force pressing against the plate to ensure mechanical equilibrium. In the absence of interfacial adhesion ($\gamma = 0$), $F = pc^2$ or $\Phi = c^2$, $\theta = 0$, and the mechanical response $c(p)$ follows Eq. (8) with $c > 0$. As the already strained

Table 1 Normalized variables

	Physical variables	Normalized variables
Geometrical parameters	$\boldsymbol{w}$ = blister profile (m) $\boldsymbol{w_0}$ = blister height (m) $\boldsymbol{a}$ = membrane radius (m) $\boldsymbol{c}$ = radius of contact circle (m) $\boldsymbol{h}$ = membrane thickness (m) $\boldsymbol{r}$ = radial distance (m) $\boldsymbol{\psi}$ = profile gradient	$w = \boldsymbol{w}/\boldsymbol{h}$ $w_0 = \boldsymbol{w_0}/\boldsymbol{h}$ $c = \boldsymbol{c}/\boldsymbol{a}$ $r = \boldsymbol{r}/\boldsymbol{a}$ $\psi = \frac{dw}{dr} = \left(\frac{\boldsymbol{a}}{\boldsymbol{h}}\right)\frac{d\boldsymbol{w}}{d\boldsymbol{r}} = \frac{\boldsymbol{a}}{\boldsymbol{h}} \times \boldsymbol{\psi}$
Material parameters	$\boldsymbol{\nu}$ = Poisson's ratio $\boldsymbol{E}$ = elastic modulus (N·m^{-2}) $\boldsymbol{\gamma}$ = interfacial adhesion energy (J m^{-2}) $\boldsymbol{\sigma}$ = tensile membrane stress (N·m^{-2})	$\gamma = \boldsymbol{\gamma}\left[\frac{6(1-\boldsymbol{\nu}^2)\boldsymbol{a}^4}{\boldsymbol{E}\boldsymbol{h}^5}\right]\sigma = \boldsymbol{\sigma}\left[\frac{12(1-\boldsymbol{\nu}^2)\boldsymbol{a}^2}{\boldsymbol{E}\boldsymbol{h}^2}\right]$
Mechanical loading	$\boldsymbol{F}$ = external force (N)	$F = \boldsymbol{F}\left[\frac{6(1-\boldsymbol{\nu}^2)\boldsymbol{a}^2}{\pi\boldsymbol{E}\boldsymbol{h}^4}\right]$
	$\boldsymbol{p}$ = applied pressure (N·m^{-2})	$p = \boldsymbol{p}\left[\frac{6(1-\boldsymbol{\nu}^2)\boldsymbol{a}^4}{\boldsymbol{E}\boldsymbol{h}^4}\right]$
	$\boldsymbol{\varepsilon}$ = Engineering strain	$\Phi = \frac{F}{p} = \frac{\boldsymbol{F}}{\pi\boldsymbol{a}^2\boldsymbol{p}}$
	$\boldsymbol{U}$ = energy terms (J)	$\varepsilon = \boldsymbol{\varepsilon}\left(\frac{\boldsymbol{a}}{\boldsymbol{h}}\right)^2$
	$\boldsymbol{G}$ = Strain energy release rate (J m^{-2})	$U = \boldsymbol{U}\left[\frac{12(1-\boldsymbol{\nu}^2)\boldsymbol{a}^3}{\pi\boldsymbol{E}\boldsymbol{h}^5}\right]$ $G = \boldsymbol{G}\left[\frac{6(1-\boldsymbol{\nu}^2)\boldsymbol{a}^4}{\boldsymbol{E}\boldsymbol{h}^5}\right]$

membrane makes contact with the plate, the inner rim of the annulus moves into the contact, and a residual strain ε_0 is locked up at the interface. Increase in c stretches the shrinking freestanding annulus further. The residual stress $\sigma_0(r)$ is a monotonic increasing function of r and continuous at $r=c$, and reaches a maximum equal to the freestanding annular stress, $\sigma=\sigma_0$ at $r=c$. No slippage is assumed at the membrane–plate interface. Depressurization deflates the blister along BAO reversibly, and the elastic energy due to the locked up strain returns to the freestanding annulus. No hysteresis is expected in the loading–unloading process. To account for interfacial adhesion ($\gamma>0$), the intersurface attraction is taken to have zero range such that adhesion occurs only when the membrane makes intimate contact with the plate. As the contact expands, the contact angle remains zero with $\theta=0$, as the blister is supported by the applied pressure. The resultant force on the plate is found by a simple vertical force balance. The mechanical response $c(p)$ traces the same path AB in Fig. 2 during loading as if no adhesion is present. Depressurization leads a different path, resulting in a hysteresis.

2.3 Delamination by Depressurization. Before deriving the delamination trajectory, it is necessary to establish the energy balance. The strain energy release rate is given by [8]

$$G=\sigma h\left(\frac{\theta^2}{2}\right)+\frac{E.h}{1-\upsilon^2}(\varepsilon-\varepsilon_0)^2 \tag{9}$$

where $\boldsymbol{\varepsilon}$ is the strain in the freestanding annulus, and $\boldsymbol{\varepsilon_0}$ the residual stress at the contact edge. The first term corresponds to the potential energy due to the applied pressure, and the second term is the elastic energy due to the annular strain subtracted by the locked-up strain. It is apparent that $\boldsymbol{\varepsilon_0}$ has a negative contribution to $\boldsymbol{G}$, as the annular membrane moves into the contact circle locking up the stored elastic energy. Mechanical equilibrium is established when the energy balance $\boldsymbol{G}=\boldsymbol{\gamma}$ is satisfied with $\boldsymbol{\gamma}$ the interfacial adhesion energy. Equation (9) can be recast as

$$\gamma=f_1\times P^{4/3}+6\times(f_2\times P^{2/3}-\varepsilon_0)^2 \tag{10}$$

with $f_1(c,\Phi)=\dfrac{1}{12^{1/3}}\times\dfrac{(c^2-\Phi)^2}{2c^2}\times(1+c^2-4\Phi+2\Phi^2\zeta^{-2})^{-1/3}$

and $f_2(c,\Phi)=\dfrac{1}{4\times 18^{1/3}}\times(1+c^2-4\Phi+2\Phi^2\zeta^{-2})^{1/3}$

The constitutive relation, $p(c, w_0)$, for a fixed γ can be found by solving Eq. (10) in a self-consistent manner. Upon pressurization along OAB, $\boldsymbol{\theta}=0$, $\boldsymbol{\varepsilon}=\boldsymbol{\varepsilon_0}$, and $\boldsymbol{G}=0$. The deformed membrane is here fully supported by p.

Depressurization along path BCD in Figs. 2 and 3 does not lead to an immediate shrinkage of the contact area but a reducing blister volume and an increasing θ in turn. At C, $\theta_C>0$ and $0<G_C<\gamma$. The coupled adhesion line force at the contact edge and the applied pressure now maintain the contact area ($c=$ constant) at the expense of the collapsing blister profile. At D, G finally reaches γ to trigger delamination. Along DHP, the energy balance $G=\gamma$ is satisfied, and the contact further diminishes. The residual stress distribution $\sigma_0(r)$ remains intact within $0\le r\le c$, but is no longer continuous at the contact edge, $\sigma_0(c)\neq\sigma(c)$. At P, $(\partial c/\partial p)\to\infty$ at c^* and p^*. Any further decrease in p ($<p^*$) deviates from the energy balance, leading to "pull-off" when the contact shrinks spontaneously from c^* to 0, and the membrane detaches from the plate. The loading (OAB) and unloading (BCDHP) processes give rise to a hysteresis when energy is dissipated due to the changing debonding angle. In the special case of loading–pressurization to an initial contact radius

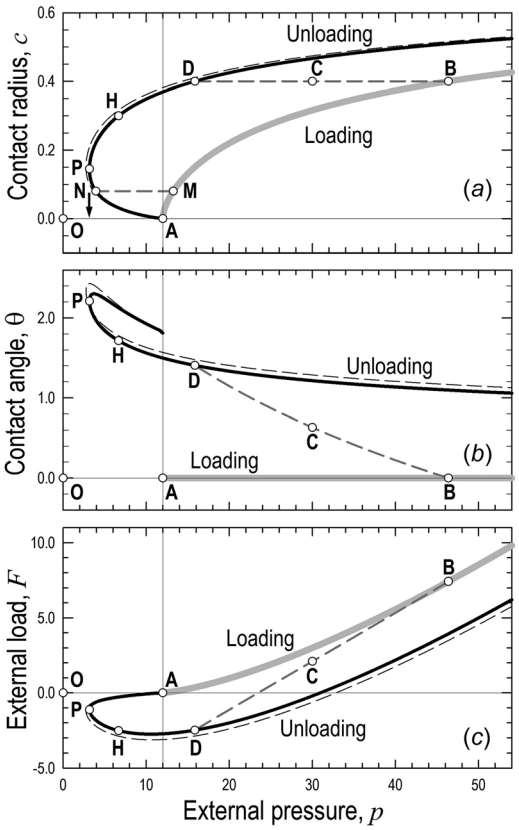

Fig. 2 Constrained blister test for adhesion energy $\gamma=5$ and plate separation $w_0=1$. There are two possible loading (gray solid) and unloading (dark solid) paths: (i) OAB-BCD-DHP with "pull-off" at P, or, (ii) OAM-MN with "pull-off" at N. (*a*) Contact radius, (*b*) contact angle, and (*c*) balancing force on the constraining plate, as a function of applied pressure. If the residual stress retained within the contact circle is ignored, the unloading curve is replaced by the thin dark dashed curve, which almost coincides with the dark solid curve here.

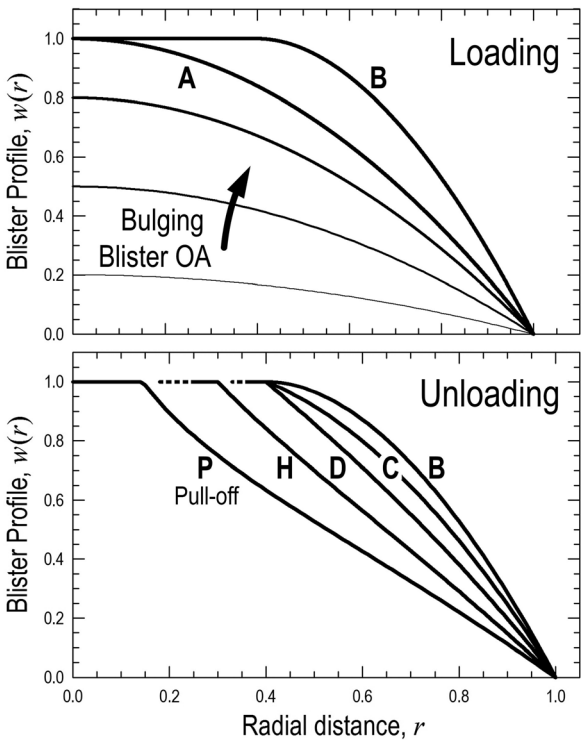

Fig. 3 The changing blister profile during loading (top) and unloading (bottom) based on Fig. 2. The flattened curve at $w=w_0=1$ corresponds to the constraining plate. Along BCD the contact radius remains constant, but the contact angle increases.

$c < c^*$ along path OAM, subsequent depressurization traverses MN with a constant c, before "pull-off" occurs at N without any gradual shrinkage of contact. Loading–unloading hysteresis now follows OAMN.

Figure 4 shows $c(p)$ for a range of adhesion energy and $w_0 = 1$. Delamination path DHP is identical to the same path in Figs. 2 and 3. In weak interfaces with $\gamma < \gamma^\dagger = 9.98$, "pull-off" occurs at positive pressure or $p^* > 0$. In case of $\gamma^\dagger$, "pull-off" occurs at $P^\dagger$ with $p^* = 0$ and $c^* = 0.2060$. In strong interfaces with $\gamma > \gamma^\dagger$, suction with $p^* < 0$ is necessary to detach the membrane. The "pull-off" locus, $c^*(p^*)$, along $APP^\dagger P'$, is where all $c(p)$ curves terminate. Figures 5(*a*) and 5(*b*) show the $p^*(\gamma)$ and $c^*(\gamma)$ for a range of w_0. Strong interface requires smaller p^* to detach the membrane at larger c^*. Should the plate be placed further away from the membrane, a larger p^* is expected. Figure 5(*c*) shows $c^*(p^*)$ for a range of w_0. For any w_0, $p^* = 0$ always requires $c^* = 0.2060$.

3 Discussion

It is worthwhile to compare the present model with the related literature. There are a number of similarities with the Johnson–Kendall–Roberts (JKR) model [15] for adhesion of elastic solid spheres with radius, R. The free membrane blister prior to contacting the constraining plate resembles the geometry of the JKR spheres, and both models assume a planar contact area. According to Maugis' interpretation [16,17], a change in the external load, P, from P_1 to P_2 does not instantly lead to the equilibrium configuration along the energy balance ($G = \gamma$), but a more tortuous path. Increasing P raises the approach distance, δ, yet a remains constant. The behavior then strictly follows the Hertz theory with $\delta = a^2/R$ as if no adhesion is present. Once final load P_2 is reached and held constant, δ and a will eventually move to the equilibrium configuration. On the other hand, decrease in load reduces δ but leaves a unchanged. With P_2 held constant, (δ, a) move to equilibrium. Maugis' model thus leads to a loading–unloading hysteresis. In the present work of membrane adhesion, the predicted behavior is quite consistent with the JKR model. The loading–pressurization expands the contact circle but $\theta = 0$ as if $\gamma = 0$, in reminiscent of the Hertz contact during the JKR-loading. Upon unloading–depressurization, θ increases but a remains constant until the energy balance is satisfied, in parallel to the JKR-unloading. Other similarities include the "pull-off" instability and the nonzero critical contact radius. A distinct difference is that the "pull-off" force depends only on the sphere radius in JKR, but both radius and film thickness in the present model.

In our previous work [10], a circular diaphragm clamped at the periphery adheres to the planar surface of a cylindrical punch. The cross section is essentially the same as Fig. 1, though the confined delamination is driven by a tensile force on the punch rather than a uniform pressure. "Pull-off" is found to be $c^* = 0.1945$, which is consistent with $c^* = 0.2060$ in the present work (c.f. Fig. 5(*c*)). In the punch model, the membrane is initially in full contact with the punch prior to delamination and is therefore free of any residual stress within the contact circle. The present model requires the membrane to be strained within the contact circle.

In Xu's model [11], membrane in contact with the constraining plate is taken to be stress free based on $(\partial w/\partial r)_{r<c} = 0$, and all elastic energy is stored in the freestanding annulus in both the loading and unloading processes. Williams [8] determined the strain energy release rate due to residual stress within the contact area in the absence of adhesion and discussed the necessity of zero contact angle during loading. The present work accounts for coupled residual stress and adhesion in the contact area. It is possible to modify our model to accommodate for such approximation that the membrane stress is taken to be uniform and continuous at $r = c$. Substituting $\boldsymbol{\varepsilon} = \boldsymbol{\varepsilon_0}$ in Eq. (9), the strain energy release rate becomes $\boldsymbol{G = \sigma h}\,(1 - \cos\boldsymbol{\theta})$ for a finite angle $\boldsymbol{\theta}$, which is essentially the Young–Dupré equation [18]. Equation (10) becomes

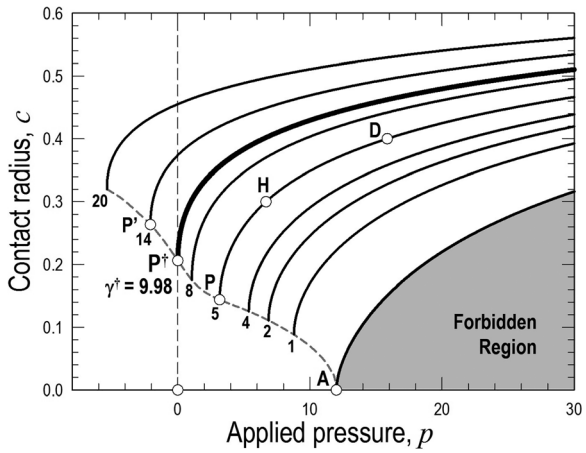

Fig. 4 Contact radius as a function of applied pressure for $w_0 = 1$ and a range of adhesion energy. The lowest curve indicates loading with $\theta = 0$ or unloading with $\gamma = 0$. The forbidden area requires $\theta < 0$ and is nonphysical. Curve DHP with $\gamma = 5$ corresponds to that shown in Figs. 2 and 3. The thick black curve is a special case with $\gamma^\dagger = 9.98$ and pull-off occurs when the "pull-off" pressure reduces to zero. "Pull-off" for $\gamma = 14$ occurs at P′ with a suction. All curves terminates at "pull-off" where $(\partial c/\partial p) \to \infty$, and the locus is shown as gray dashed curve $APP^\dagger P'$.

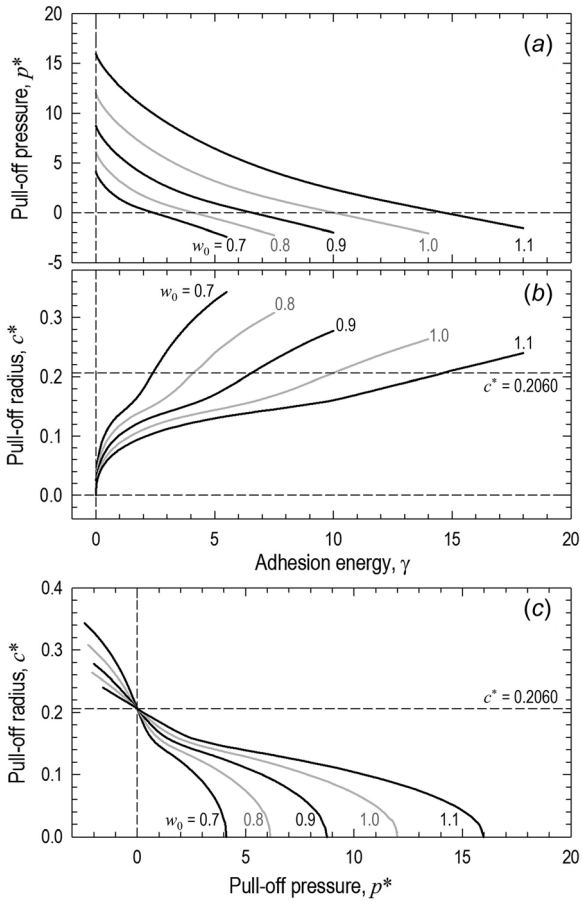

Fig. 5 Relations of "pull-off" parameters for a range of plate-substrate gap w_0. (*a*) Critical pressure and (*b*) radius as functions of adhesion energy. When adhesion is stronger than a specific threshold depending on w_0, suction is necessary to detach the membrane. (*c*) Critical contact radius as a function of critical pressure. For any w_0, $p^* = 0$ always leads to $c^* = 0.2060$.

$$\gamma = f_1 \times p^{4/3} \tag{11}$$

Figure 2 shows the loading–unloading process using Eq. (11) as a thin dark dashed curve which almost coincides with the exact calculation for $w_0 = 1$ and $\gamma = 5$. Slightly larger p^* and c^* are expected at "pull-off." It is also worth to mention that models by Plaut et al. [9] and Xu assume loading and unloading to follow the energy curve and does not show the loading–unloading hysteresis as in the present model.

Long et al. [13,14] modeled a hyperelastic blister under large pressure. The membrane is blown into truncated sphere with a large meridian angle as large as 90 deg that makes adhesion contact with the plate. The loading–pressurization assumes $\theta = 0$, and unloading–depressurization shows an initial constant contact radius and an increasing θ. The 3D stresses and strains in cylindrical coordinates are computed numerically. The "pull-off" parameters are also deduced based an energy balance. The general features and trends of the interrelationships between measurable quantities are consistent with the present model, e.g., monotonic decreasing functions of $p^*(\gamma)$ and $c^*(\gamma)$. It is, however, difficult to compare the two models, since two different normalization schemes are used. The present model presents a limiting extreme of the large deformation model and provides an analytical solution to the experimentalists working with linear elastic membranes under small strain.

As a final remark, the assumption that plate bending is ignored in our theoretical model deserves further discussion. In linear elasticity, bending dominates at small deformation when the blister height is comparable to membrane thickness, or $\boldsymbol{w_0 \sim h}$. However, many practical membranes (e.g., biomembranes and lipid bilayers in cells and liposomes) do not strictly follow this rule because of the high degree of flexibility. Such films virtually conform to the substrate topology under membrane stretching in a practical sense. To facilitate description of complex biomembrane without involved solid mechanics, a representative pseudo elastic modulus, or areal expansion modulus, is adopted such that plate bending can be ignored at all times. A strictly plate bending model is mathematically involved. Moreover, practical experiments always operate in a deformation regime governed by membrane stretching. A comprehensive model involving mixed bending-stretching leads to an analytical solution, if at all possible, which will be challenging for experimentalists to adopt for data analysis.

4 Conclusion

A linear elastic model is built for a constrained blister test where the clamped membrane adheres, delaminates, and detaches from the constraining plate. The adhesion–delamination process and the relations between the plate-membrane gap, applied pressure, blister height, contact radius, and adhesion energy, as well as the "pull-off" thresholds, are derived.

Acknowledgment

This work was supported by National Science Foundation Grant No. CMMI # 1232046. Any opinions, findings, and conclusions or recommendations expressed in this material are those of the authors and do not necessarily reflect the views of the National Science Foundation.

References

[1] Dannenberg, H., 1961, "Measurement of Adhesion by a Blister Model," J. Appl. Polym. Sci., **5**(14), pp. 125–134.
[2] Wan, K.-T., and Mai, Y. W., 1995, "Fracture-Mechanics of a New Blister Test With Stable Crack-Growth," Acta Metall. Mater., **43**(11), pp. 4109–4115.
[3] Wan, K.-T., 2000, "A Novel Blister Test to Investigate Thin Film Delamination at Elevated Temperature," Int. J. Adhes. Adhes., **20**(2), pp. 141–143.
[4] Chang, Y. S., Lai, Y. H., and Dillard, D. A., 1989, "The Constrained Blister—A Nearly Constant Strain Energy Release Rate Test for Adhesives," J. Adhes., **27**(4), pp. 197–211.
[5] Lai, Y. H., and Dillard, D. A., 1990, "An Elementary Plate Theory Prediction for Strain Energy Release Rate of the Constrained Blister Test," J. Adhes., **31**(2–4), pp. 177–189.
[6] Lai, Y. H., and Dillard, D. A., 1990, "Numerical Analysis of the Constrained Blister Test," J. Adhes., **33**(1–2), pp. 63–74.
[7] Napolitano, M. J., Chudnovsky, A., and Moet, A., 1988, "The Constrained Blister Test for the Energy of Interfacial Adhesion," J. Adhes. Sci. Technol., **2**(1), pp. 311–323.
[8] Williams, J. G., 1997, "Energy Release Rates for the Peeling of Flexible Membranes and the Analysis of Blister Tests," Int. J. Fract., **87**(3), pp. 265–288.
[9] Plaut, R. H., White, S. A., and Dillard, D. A., 2003, "Effect of Work of Adhesion on Contact of a Pressurized Blister With a Flat Surface," Int. J. Adhes. Adhes., **23**(3), pp. 207–214.
[10] Wan, K.-T., and Julien, S. E., 2009, "Confined Thin Film Delamination in the Presence of Intersurface Forces With Finite Range and Magnitude," ASME J. Appl. Mech., **76**(5), p. 051005.
[11] Xu, D., and Liechti, K. M., 2011, "Analytical and Experimental Study of a Circular Membrane in Adhesive Contact With a Rigid Substrate," Int. J. Solids Struct., **48**(20), pp. 2965–2976.
[12] Flory, A. L., Brass, D. A., and Shull, K. R., 2007, "Deformation and Adhesive Contact of Elastomeric Membranes," J. Polym. Sci. Part B, **45**(24), pp. 3361–3374.
[13] Long, R., Shull, K. R., and Hui, C.-Y., 2010, "Large Deformation Adhesive Contact Mechanics of Circular Membranes With a Flat Rigid Substrate," J. Mech. Phys. Solids, **58**(9), pp. 1225–1242.
[14] Long, R., and Hui, C.-Y., 2012, "Axisymmetric Membrane in Adhesive Contact With Rigid Substrates: Analytical Solutions Under Large Deformation," Int. J. Solids Struct., **49**(3–4), pp. 672–683.
[15] Johnson, K. L., Kendall, K., and Roberts, A. D., 1971, "Surface Energy and the Contact of Elastic Solids," Proc. R. Soc. London, Ser. A, **324**(1558), pp. 301–313.
[16] Maugis, D., and Barquins, M., 1978, "Fracture Mechanics and the Adherence of Viscoelastic Bodies," J. Phys. D: Appl. Phys., **11**(14), pp. 1989–2023.
[17] Maugis, D., 2000, *Contact, Adhesion and Rupture of Elastic Solids*, Springer, New York.
[18] Adamson, A. W., 1997, *Physical Chemistry of Surfaces*, 6th ed., Wiley-Interscience, New York.